Transient Free-Surface Flows in Injection Mold Filling

Advancing and colliding flow fronts are important fluid mechanical problems in injection mold filling. These are small-scale, transient free-surface flows with a significant impact on the molecular orientation of molded parts. This paper describes a numerical technique for the simulation of transient free-surface flows. The algorithm combines a Galerkin/finite-element discretization of the governing equations with a predictor-corrector scheme for integration in time, and determines simultaneously the flow field and the free surface at every time step. The method is applied to the start-up of a fluid flow initially at rest and impingement of two flow fronts to form a weldline. Comparison of simulation with available experiments on the start-up problem shows very good agreement. Numerical tracking of fluid elements clarifies various aspects of flow-induced deformation of the material.

H. Mavridis, A. N. Hrymak, J. Vlachopoulos
Department of Chemical Engineering
McMaster University
Hamilton, Ontario, Canada L8S 4L7

Introduction

Mold filling operations in polymer processing involve a transient free-surface flow in complex geometries. A key fluid mechanical feature is the flow rearrangement behind the advancing front, described by Rose (1961) as "fountain flow": the streamlines of a fluid advancing in a tube (or between parallel plates) appear like a fountain when viewed from a frame of reference moving with the flow front. The transition region extends a distance of the order of the gapwidth behind the front and has little effect on global quantities such as the pressure drop or the filling time. However, it has a marked impact on a microscopic scale; flow-induced deformation in the complex shear and elongational region behind the front and the rolling-type motion caused by fountain flow affect the orientation of polymer chains and fillers near the molded article surface.

The implications of fountain flow in injection molding have been known at least since the experimental investigations of Ballman and Toor (1960) on birefringence of molded parts. The visualization experiments of Schmidt (1974) with color tracers provided detailed information about the kinematics of the flow. Tadmor (1974) did a semiquantitative study of the effect of the flow front on molecular orientation by modeling the front region as a planar stagnation flow. Tadmor's model was adopted by White and Dietz (1979) for the prediction of birefringence distributions.

Theoretical attempts to investigate the fluid mechanics of fountain flow have considered steady, isothermal flow in straight-walled channels. Under these assumptions, the problem can be solved in the steady state. A summary of previous work and detailed finite-element calculations with Newtonian and shear-thinning fluids in planar and axisymmetric geometries have been given by the present authors in a recent paper (Mavridis et al., 1986a). The effect of fountain flow on the deformation of fluid elements was investigated by tracking material elements, simulating the formation of V shapes photographed by Schmidt (1974) (Mavridis et al., 1986b). Similar results were obtained by Coyle et al. (1987) and Chu et al. (1987).

Behrens (1983) and Behrens et al. (1987) examined the transient fountain flow in a tube using the finite-element method. The calculated evolution of the front tip-contact line distance showed good agreement with experimental measurements.

There appears to be no theoretical fluid mechanical study of the even more interesting and intricate case of two colliding flow fronts to form a weldline. This situation arises frequently in commercial molds due to injection through multiple gates or recombination of two flow fronts divided after passage around an insert. During the impingement phase, polymer molecules are stretched and oriented parallel to the polymer-polymer interface. Depending on the local thermal conditions, this orientation may be "frozen-in," resulting in incomplete bonding and reduction in the strength of the weldline; Sang-Gook and Suh (1986) offer a recent review and analysis of the problem.

The present paper is a simulation approach to the solution of transient free-surface problems in mold filling. The numerical technique combines a Galerkin/finite-element discretization of

the governing equations with a predictor-corrector scheme for the integration in time. Efficient strategies for free surface parameterization are applied that can handle large distortions of the flow domain. The computational algorithm is fast and economical and determines simultaneously the free surface position and the flow field at every time step.

The method is applied to the transient fountain flow problem (start-up flow of a fluid initially at rest) and the collision of the two advancing flow fronts in a planar geometry (weldline formation in the gapwise direction). Numerical tracking of material elements highlights various aspects of the flow-induced deformation experienced by the fluid. Quantitative comparison of the computational results shows very good agreement with the experiments of Behrens et al. (1983, 1987) for transient fountain flow in a tube.

Governing Equations and Boundary Conditions

For an incompressible viscous fluid, the mass and momentum conservation equations in dimensionless form are:

$$\nabla \cdot v = 0 \tag{1}$$

$$Re\left(\frac{\partial v}{\partial t} + v \cdot \nabla v\right) = \nabla \cdot \sigma + S^{-1} g \tag{2}$$

Variables are made dimensionless with a characteristic velocity U, length L, and viscosity μ. The total stress tensor, $\sigma = -PI + \tau$, is scaled with $\mu U/L$. The Reynolds number is $Re \equiv \rho UL/\mu$ and the Stokes number $S \equiv \mu U/\rho g L^2$, where ρ is the density and g the gravitational acceleration. Under typical mold filling conditions Re and S^{-1} are both very small (i.e., negligible convective and gravitational effects).

Appropriate boundary conditions require the specification of two scalar boundary conditions on every portion of the flow boundary. A velocity field satisfying Eq. 1 and the initial shape of the free surface must be specified as initial conditions for transient flows.

In fully developed flow regions, symmetry lines, and at the wall, the boundary conditions are: fully developed velocity profile, symmetry conditions, and no slip, respectively. At the free surface a local force balance provides the following boundary conditions:

$$n \cdot \sigma = \frac{2H}{Ca} n - P_a n \tag{3a}$$

where n is the outward unit vector normal to the surface, $2H$ is the mean surface curvature, and P_a the ambient pressure (usually set to zero as the pressure datum). Ca is the capillary number defined as the ratio of viscous to surface tension forces, $Ca \equiv \mu U/\gamma$. In injection molding of molten polymers, the capillary number is large and Eq. 3a reduces to the no-traction condition:

$$n \cdot \sigma = 0 \tag{3b}$$

Another boundary condition arises at the free surface from mass conservation considerations: a free surface is a material surface and no fluid particle crosses it. For a point x at the free surface this condition is expressed as

$$n \cdot v = n \cdot \left(\frac{\partial x}{\partial t}\right)_F \tag{4}$$

The contact line, where the free surface intersects a solid wall, poses a special problem and is discussed below.

Contact line motion

Complications arise at the contact line: when the no-slip boundary condition is applied at the wall up to the contact line, a stress singularity results (stresses increase without bound as the contact line is approached). Singular stresses, although aphysical, can be tolerated as long as they are integrable, i.e., the total force exerted on the fluid remains finite. When the contact line does not move (static contact line) the singularity is integrable (Michael, 1958). For a moving contact line, the singularity is nonintegrable when the contact angle is less than 180° (Huh and Scriven, 1971; Dussan, 1979). Pismen and Nir (1982), who obtained a perturbation solution in the vicinity of the contact line for the case of a liquid advancing into an inviscid medium, reported an integrable singularity for a 180° contact angle. In this work, only viscous effects are taken into account and the contact angle at a moving contact line is required to be 180°; therefore, the singularity is integrable and there is no need to remedy the situation, for example with a slip boundary condition.

There remains a difficulty in treating the apparent motion of the contact line, especially for transient flows. Consider the start-up flow problem, where the initial free surface is perpendicular to the wall, $ABCD$ at time t_0 in Figure 1. As the flow begins the free surface deforms and the contact angle increases (time t_1). In the numerical algorithm the position of the contact line is fixed up to the time that the contact angle becomes 180°. At this time the condition of a fixed contact line position is replaced by a 180° contact angle condition, and the contact line is allowed to move. The mechanism implied by these conditions is that of a rolling motion of the fluid over the solid surface. It should be noted that the motion of the contact line is apparent, i.e., there is no slip. A different material particle occupies the contact line position at every instant, and the contact line appears to move as new material reaches the wall from the free surface, as indicated in Figure 1.

The above requirements for the contact line motion provide the necessary condition for the determination of the contact line position. Other workers (Behrens, 1983, and Behrens et al.,

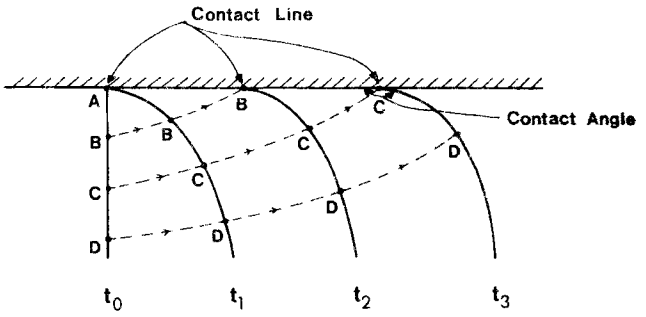

Figure 1. Contact line motion over a solid surface.

1987 for transient flows; Viriyayuthakorn and Deboo, 1983, for steady flows) do not impose explicitly a condition at the contact line but determine its position implicitly; the kinematic condition, Eq. 4, is imposed at the free surface and the contact line is determined at the intersection of the extrapolated free surface with the wall. This implicit scheme is equivalent to that used here, i.e., combination of the kinematic boundary condition with no slip at the contact line directly yields the present scheme, as will be shown below.

Consider, for example, a fluid displacing a gas over a flat solid surface, parallel to the x direction, as shown in Figure 2. If we parametrize the free surface as $y = h(x)$, the outward unit vector normal to the surface is:

$$\boldsymbol{n} = \left[1 + \left(\frac{\partial h}{\partial x}\right)^2\right]^{-1/2}\left[-\boldsymbol{i}\left(\frac{\partial h}{\partial x}\right) + \boldsymbol{j}\right] \tag{5}$$

and the kinematic conditions, Eq. 4, can be written as:

$$-\left(\frac{\partial h}{\partial x}\right)u + v = -\left(\frac{\partial h}{\partial x}\right)\frac{\partial x}{\partial t} + \frac{\partial h}{\partial t} \tag{6a}$$

At the contact line $u = v = 0$ (no slip) and $\partial h/\partial t = 0$ (straight wall). Then Eq. 6a becomes:

$$\left(\frac{\partial h_{CL}}{\partial x}\right)\cdot\left(\frac{\partial x_{CL}}{\partial t}\right) = 0 \tag{6b}$$

From Eq. 6b we notice that:

1. When the contact angle is less than 180° ($\partial h_{CL}/\partial x \neq 0$) then the contact line does not move ($\partial x_{CL}/\partial t = 0$)
2. For the contact line to move ($\partial x_{CL}/\partial t \neq 0$) the contact angle must be 180° ($\partial h_{CL}/\partial x = 0$)

The above conditions result from purely kinematic considerations at the contact line, combined with the no-slip hypothesis. They are appropriate when surface tension effects are insignificant, which is the case for the problems examined in this paper.

Numerical Simulation

For transient free-surface flows the position and shape of the flow front is not only unknown in space but also evolves in time. Accuracy in the determination of the free-surface shape is crucial for the success of the simulation, especially in the limit of creeping flow where the time dependence is implicit and enters only through the kinematic condition, Eq. 4, at the free surface. The flow domain not only deforms in shape but also its size expands with time, since there is no outflow region.

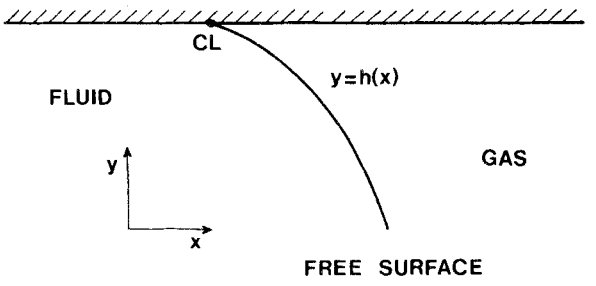

Figure 2. A solid-fluid-gas contact line.

The method employed here is a version of the *u-v-p-h* formulation of the Navier-Stokes system introduced by Saito and Scriven (1981), generalized by Kistler and Scriven (1983), and extended to transient flows by Kheshgi and Scriven (1984). A similar method has also been applied by Keunings (1986) in the context of viscoelastic flows. The basics of the formulation and an efficient strategy for free-surface parameterization, especially useful in transient flows, are described below.

Free-surface parametrization

The free surface is represented by piecewise quadratic line segments, each of which forms one side of an isoparametric 9-node quadrilateral element. A free-surface segment is defined uniquely by the coordinates of three nodal points, two end points and the midside point. Every free-surface node $\boldsymbol{x}_F^i$ moves along a predefined spine, a straight line that is characterized by a base point $\boldsymbol{x}_B^i$ and a unit vector $\boldsymbol{e}^i = \boldsymbol{i}\cos\delta^i + \boldsymbol{j}\sin\delta^i$, where $\cos\delta^i$, $\sin\delta^i$ are the direction cosines of $\boldsymbol{e}^i$. The position of $\boldsymbol{x}_F^i$ is determined as the distance along the spine, i.e.,

$$\boldsymbol{x}_F^i = \boldsymbol{x}_B^i + h^i\,\boldsymbol{e}^i \tag{7}$$

If $\boldsymbol{x}_F^{i-1}$, $\boldsymbol{x}_F^i$, $\boldsymbol{x}_F^{i+1}$ are the three nodes that define a free-surface segment, the free surface is represented as:

$$\boldsymbol{x} = \sum_{i-1}^{i+1} \boldsymbol{x}_F^j\,\phi^j(\xi, \eta = 1) \tag{8}$$

where $\phi^j(\xi, \eta)$ are biquadratic basis functions that map isoparametrically the nine-node element onto the standard ξ-η square, and $\eta = 1$ is the side corresponding to the free-surface segment.

In general, there are two position parameters corresponding to every free-surface node $\boldsymbol{x}_F^i$:h^i that is associated with distance, and δ^i that is associated with orientation. The δ^i parameters corresponding to free-surface end points are fixed, while those corresponding to midside nodes enter the set of unknowns. The latter δ^i are determined on the requirement that the midside node be located at the midpoint of the free-surface arc. The mathematical expression of this requirement is as follows. Assume that the free-surface segment is mapped on the $-1 \le \xi \le 1$, $\eta = 1$ side of the standard ξ-η square. The corner and midside nodes are at $\xi = -1$, 1 and 0, respectively. The differential arc length ds is:

$$\mathrm{ds} = \sqrt{x_\xi^2 + y_\xi^2}\,|_{\eta=1}\,d\xi \tag{9}$$

and the condition that the midside node is at the midpoint of the arc is:

$$\int_{\xi=-1}^{\xi=0} \mathrm{ds} = \int_{\xi=0}^{\xi=1} \mathrm{ds}$$

or

$$\int_{-1}^{0} \sqrt{x_\xi^2 + y_\xi^2}|_{\eta=1}\,d\xi = \int_{0}^{1} \sqrt{x_\xi^2 + y_\xi^2}|_{\eta=1}\,d\xi \tag{10}$$

The changing midside spine direction is especially necessary in transient flows where the free surface changes drastically. In these cases constant-directed spines may result in badly distorted or even singular elements. It must be noted that moving

the midside node away from the midpoint and toward the corner of the element is standard practice in structural mechanics for modeling singular stress behavior at the corner node (Banthia, 1985).

The usefulness of having a variable midside spine direction is shown in Figure 3, which is a plot of the evolution of the free-surface segment near the wall, for the transient fountain flow problem. The corner node moves along the constant-direction spine (straight trajectory) while the midside spine direction changes (curved trajectory) so that the midside node remains always at the midpoint and the element is well shaped.

For a free surface represented by NF segments (element sides) there are $2NF + 1$ h^i variables (as many free surface nodes) and NF δ^i variables. Interior nodes are located as explicit functions of free-surface node position so that the finite-element grid deforms in proportion to the free-surface motion. More details and illustrative examples are given elsewhere (Kistler, 1984; Kistler and Scriven, 1983).

Galerkin/Finite-element formulation

The finite-element approximation of the velocity and pressure field is:

$$v = \sum_i v^i \phi^i(\xi, \eta) \qquad P = \sum_i P^i \pi^i(\xi, \eta) \tag{11}$$

where v^i, P^i are nodal variables, and $\phi^i(\xi, \eta)$ and $\pi^i(\xi, \eta)$ are the corresponding basis functions. Elements used in this work are the nine-node quadrilateral and six-node triangular isoparametric element with C^0-P^2 approximation for the velocity and C^0-P^1 for the pressure.

The Galerkin principle is invoked to discretize the governing equation in space. The vector of unknowns is:

$$X^T = [V^T, P^T, h^T, \delta^T] \tag{12}$$

and the corresponding residuals

$$R^T = [R_m^T, R_c^T, R_k^T, R_\delta^T] \tag{13}$$

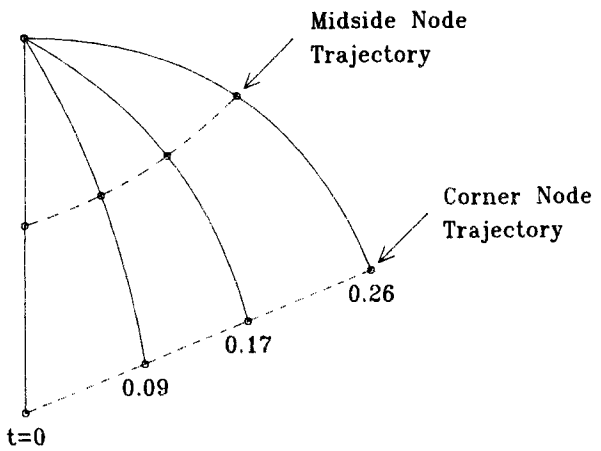

Figure 3. Evolution of corner free-surface segment (transient fountain flow).

where R_m is the momemtum residuals, R_c the continuity residuals, R_k the kinematic residuals at the free surface, and R_δ the residuals in Eq. 10. Specifically:

$$R_m^i = \int_\Omega \left\{ Re \frac{Dv}{Dt} \phi^i + \nabla \phi^i \cdot \sigma - S^{-1} \phi^i g \right\} d\Omega - \int_{\partial\Omega} n \cdot \sigma \phi^i \, ds \tag{14}$$

$$R_c^i = \int_\Omega \nabla \cdot v \pi^i d\Omega \tag{15}$$

$$R_k^i = \int_F \left\{ n \cdot v - n \cdot \frac{\partial x}{\partial t} \right\} \phi^i(\xi, \eta = 1) ds \tag{16}$$

$$R_\delta^i = \int_{-1}^{0} \sqrt{x_\xi^2 + y_\xi^2}|_{\eta=1} \, d\xi - \int_0^i \sqrt{x_\xi^2 + y_\xi^2}|_{\eta=1} \, d\xi \tag{17}$$

The material derivative in Eq. 14 is written as

$$\frac{Dv}{Dt} = \frac{\partial v}{\partial t} + \left(v - \frac{\partial x}{\partial t} \right) \cdot \nabla v \tag{18}$$

to account for the nodal motion ($\partial x/\partial t$) in the deforming finite-element grid (Lynch, 1982; Khesghi and Scriven, 1984; Keunings, 1986).

The conditions for the contact line motion are implemented as follows. The contact angle θ is computed from

$$\theta = \cos^{-1} (n_{CL} \cdot n_w) \tag{19}$$

where n_w is the unit vector normal to the wall ($n_w = -j$ in the present case) and n_{CL} is the unit vector normal to the free surface at the corner of the element adjacent to the contact line:

$$n_{CL} = \left. \frac{-y_\xi i + x_\xi j}{(x_\xi^2 + y_\xi^2)^{1/2}} \right|_{\xi=-1,\eta=1} \tag{20}$$

When $\theta < 180°$ the h^i variable corresponding to the contact line position is fixed with an essential boundary condition. When θ becomes 180° the contact line is allowed to move and the corresponding h^i is determined on the requirement of a 180° contact angle condition, which is imposed by adding the equation

$$n_{CL} \cdot n_w = \cos (180°) \tag{21}$$

in the algebraic system to be solved.

Time integration and solution of the algebraic system

The time derivatives in the momentum and kinematic residuals, Eqs. 14 and 16, are approximated with finite differences. An Adams-Basforth predictor—trapezoid rule corrector is employed for the integration in time. The predictor-corrector scheme adjusts automatically the time step size so as to keep the time discretization error below a predefined tolerance. More details can be found in Gresho et al. (1979) and Khesghi and Scriven (1984).

At every time step the algorithm involves the solution of a nonlinear system of algebraic equations for the corrector step, with the initial guess provided by the predictor. This system is

solved with Newton-Raphson iteration, i.e.,

$$X_{new} = X_{old} - J^{-1} R|_{X_{old}} \tag{22}$$

where $J \equiv \partial R/\partial X$, the Jacobian of the global system.

Typically the Newton-Raphson iteration approached quadratic convergence, as shown in Figure 4. This figure shows that after one iteration the Euclidean norm of residuals has been reduced below 10^{-4}. Gresho et al. (1979) and Khesghi and Scriven (1984) have taken advantage of this behavior of Newton-Raphson and allowed only one iteration per step. In this work two to three iterations were required to reduce the maximum relative update below 10^{-4}. This conservative convergence criterion was imposed in order to ensure a high accuracy in the determination of the free-surface shape, which is of main interest for the problems studied.

Transient Fountain Flow

We study the start-up flow of a fluid with a free front initially at rest, in both planar and axisymmetric geometries. A diagram of the problem is given in Figure 5. Gravity and surface tension effects are neglected, so that the fluid-gas interface is initially flat and perpendicular to the walls (90° contact angle). These conditions correspond to the experiments of Behrens (1983).

For a typical simulation the finite-element grid consists of 45 elements and 199 nodes. The total number of unknowns (u, v, p, h, δ) is 412 and each time step requires 30 CPU seconds on a VAX 8600 computer.

Figure 6 shows the evolution of the contact angle and the front tip and contact line positions for transient flow in a tube. Up to the time that the contact angle becomes 180° the contact line does not move (its position is specified as an essential boundary condition). This time is predicted to be 0.2272 and the front tip position $Z_{FT} = 0.3736$ (time and position = 0.26 and 0.3508, respectively, for the planar case). Behrens et al. (1987) report an experimental $Z_{FT} = 0.4$ when the contact line begins to move. This is 7% higher than the present result, but this difference is not significant in view of the very slow initial motion of the contact line (Z_{CL} is predicted to be $8.5*10^{-3}$ when Z_{FT} becomes 0.4). When the contact angle becomes 180°, the contact line is allowed to move and the boundary condition at the contact line is changed to that of a 180° contact angle. Therefore the contact angle remains at 180° for all subsequent times. The contact line starts moving slowly and its velocity approaches asymptotically the average velocity of the fluid.

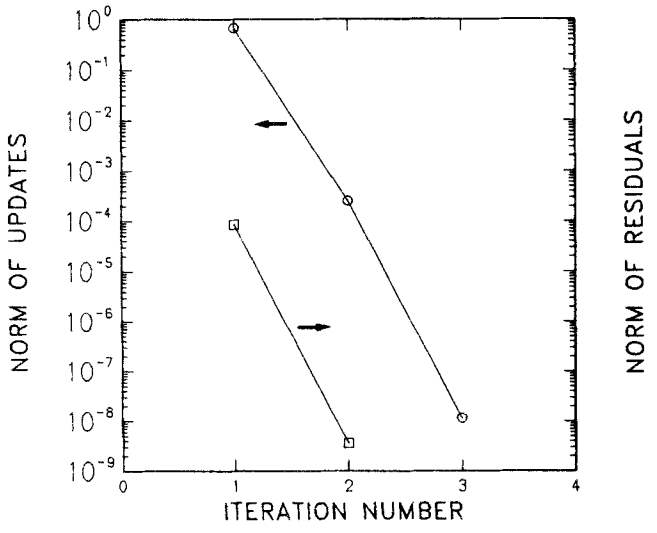

Figure 4. Behavior of Newton-Raphson iteration.

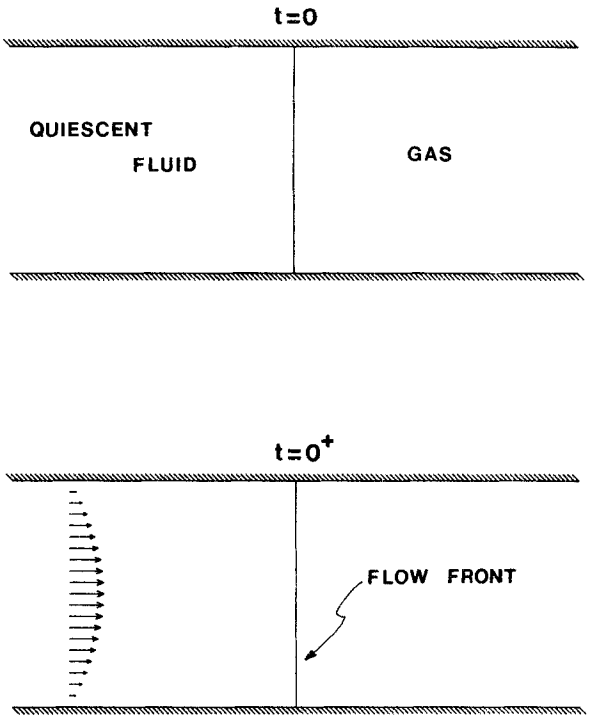

Figure 5. Transient fountain flow problem.

Similar results were found for flow in a planar geometry. Figure 7 shows the evolution of the free-surface shape. A steady state is reached in approximately three time units. After this time the flow field remains invariant with respect to a frame of reference moving with the average velocity of the fluid and the problem can be analyzed in the steady state (Mavridis et al. 1986a).

Behrens (1983) performed experiments with Newtonian fluids in tubes. Data were reported in the form of the

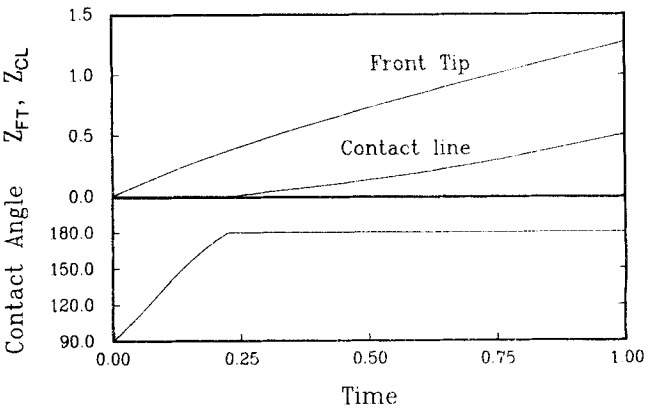

Figure 6. Evolution of contact angle and front tip and contact line positions (axisymmetric).

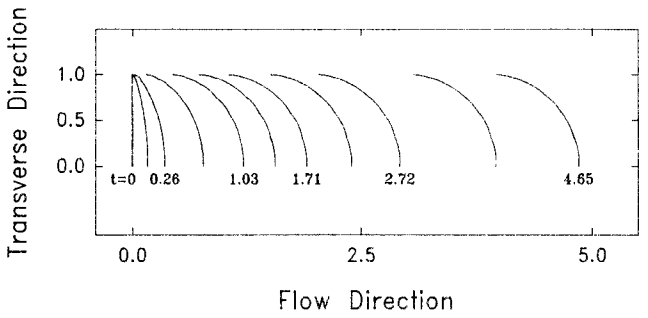

Figure 7. Evolution of flow front shape (planar).

($Z_{FT} - Z_{CL}$) difference vs. front travel (Z_{FT}). Comparison of the present simulations with Behrens' experimental data is given in Figure 8. The data symbols correspond to different experiments with polybutene, and the scatter does not correlate with process variables but merely reflects experimental error. The agreement of simulation with experiment is remarkably good. Behrens (1983) and Behrens et al. (1987) also presented simulations with a finite-element method where the free surface and the flow field were decoupled. Good agreement with the experiments was found. The predicted motion of the contact line showed slight oscillations that do not appear with the present algorithm. The major advantage of the present approach is the free-surface parameterization strategy and the coupled technique for determining simultaneously the free surface and the flow field. Coupling allows the use of the Newton-Raphson iterative scheme for the solution of the global nonlinear system of algebraic equations. The quadratic convergence of Newton-Raphson reduces considerably the computational cost.

The evolution of the finite-element grid, for the axisymmetric case, is shown in the upper part of the plots in Figure 9. This figure illustrates how the grid deforms and expands, adjusting automatically to the changing free-surface shape. As was mentioned earlier, the area of the flow domain increases since there is no outflow region. This increase was accommodated by expanding the size of the upstream elements only. The grid density in the front region, where the flow rearrangement occurs, remained nearly independent of time, thus avoiding a degradation of accuracy at large times.

The mechanism of flow front advancement can be understood better by tracking material elements, i.e., in the Lagrangian frame. We begin with rectangular material elements at zero time, as shown in Figure 9. The deformation history can be followed by tracking numerically a large number of material points along the perimeter of the fluid element as described by Mavridis et al. (1986b). Consider first the fluid element adjacent to the flow front. The evolution of its shape, shown in the lower part of the plots in Figure 9, illustrates clearly the rolling motion of the fluid over the solid surface, and how material from the flow front is deposited on the wall, giving rise to the apparent motion of the contact line. The evolution of the shape of the second element is characteristic of the deformation experienced by the fluid due to fountain flow. The faster moving material near the centerline enters the flow front region where it decelerates, spilling outward toward the walls. The fluid element is stretched and deformed into a mushroomlike shape ($t = 2.27$), forming characteristic V shapes near the wall ($t = 4.15$). The formation of the V shapes was observed in the color tracer studies of Schmidt (1974) and predicted numerically for the first time by Mavridis et al. (1986b). Similar results were found by Coyle et al. (1987) and Chu et al. (1987) with steady state analyses. Recently, Beris (1987) showed that the prediction of V-shape formation is independent of the constitutive equation and/or the isothermality condition used in the simulations. The nature of the fluid and solidification at the wall determine the actual time and length scales involved in the formation of the V shapes but do not change the overall picture qualitatively.

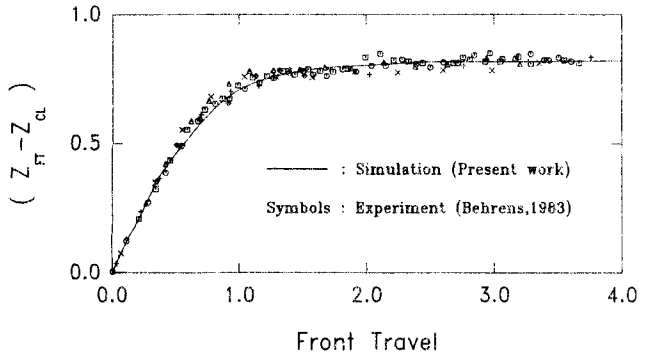

Figure 8. ($Z_{FT} - Z_{CL}$) v. front tip position Z_{FT} for transient axisymmetric fountain flow.

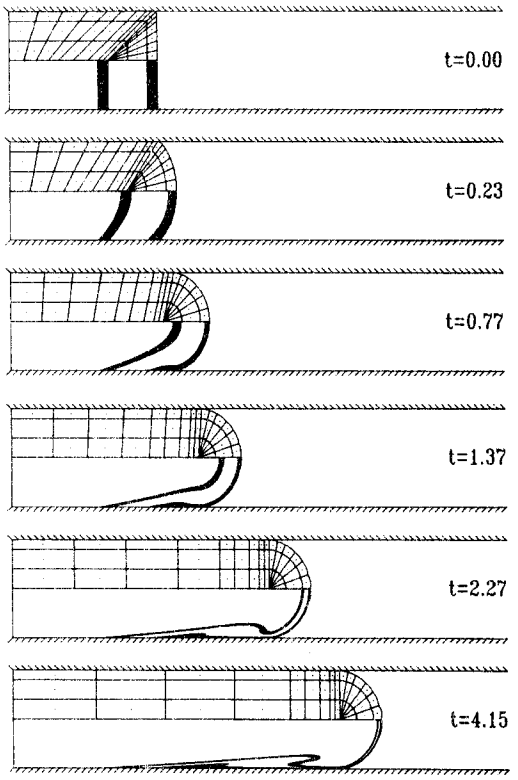

Figure 9. Evolution of finite-element grid and fluid element shapes (axisymmetric).

Colliding Flow Fronts

We consider the symmetrical impingement of two flow fronts in a parallel-plate geometry, as shown in Figure 10. Creeping Newtonian flow and constant flow rate conditions are assumed in the simulations. The problem is solved in a quarter of the flow domain, taking into account symmetry conditions.

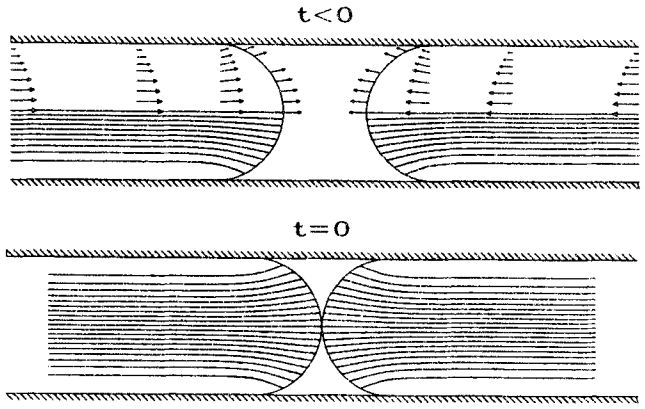

Figure 10. Colliding flow fronts.

At $t = 0$ the flow fronts meet at the centerline. The shape of the free surface, required as an initial condition, is taken from the steady state solution of the fountain flow problem. The present transient algorithm is applied to obtain the solution in time. The time required to fill the vacant space can be estimated *a priori* by dividing the area of the vacant space by the constant flow rate. This time is calculated to be 0.212 in L/U units. At this time no more flow can occur (incompressible fluid) and the algebraic system of equations is singular. The numerical algorithm stopped at $t = 0.21$, leaving a small vacant area at the surface, Figure 11. This area is the last to be filled and in practice the air trapped in it may cause an optically visible defect in the shape of a notch at the surface (Hagerman, 1973; Sang-Gook and Suh, 1986).

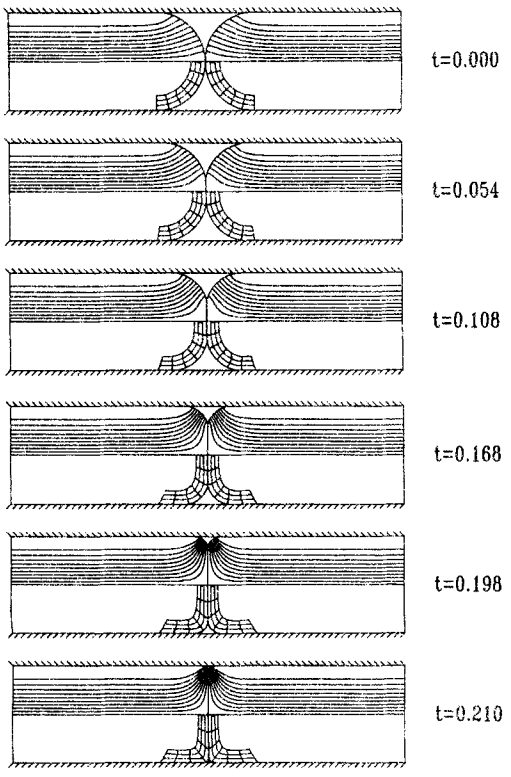

Figure 11. Evolution of instantaneous streamlines and fluid element shapes.

The evolution of the flow field is shown as a series of instantaneous streamlines in the upper part of the plots in Figure 11. At zero time the curvature of the streamlines reflects the outward motion of the fluid due to fountain flow. As the weldline forms at the centerline and develops towards the wall, the elongational component of the deformation increases and the streamlines bend parallel to the weld line. At the end the flow resembles planar stagnation flow. In fact, the planar stagnation flow model of Tadmor (1974) has frequently been used to explain the flow-induced orientation parallel to the weldline.

The impact of weldline formation on the deformation of the material was investigated by tracking numerically a gridded band of material behind the flow front. This material is already stretched due to fountain flow (observe for example the fluid element shapes near the flow front at time $t = 4.15$ in Figure 9) but we examine here the stretching induced during the impingement phase. The evolution of the fluid element shapes is shown in the lower part of the plots in Figure 11. The material elements become stretched and oriented parallel to the weldline, and stretching is more pronounced near the centerline, while near the wall shearing orients the material parallel to the wall. This is better illustrated in Figure 12, which is a magnification of the band of material immediately adjacent to the flow front. This material has already experienced the fountain-flow-induced deformation before the collision of the two fronts. Comparison of the fluid element shapes in Figure 12 and Figure 9 shows that the stretching due to fountain flow is much larger (see also Mavridis et al., 1986b). While some orientation of the material is introduced during the collision phase, it appears that fountain flow is mostly responsible for the anisotropy at weldlines of injection molded parts.

It is particularly interesting to note the actual length and time scales involved in weldline formation. For a typical case, with an average velocity $U = 0.1$ m/s and half-gapwidth $L = 10^{-3}$ m the weldline forms in 0.21 $L/U = 2.1$ ms. Experiments are difficult to perform and their analysis is a laborious off-line procedure. Numerical simulations can be of invaluable assistance, providing insight into the process, at time and length scales that are difficult to capture or reproduce experimentally.

Concluding Remarks

A comprehensive algorithm has been described for the numerical simulation of transient free surface flows encountered in injection mold filling. The technique determines simultaneously the flow field and the free surface shape and can handle deforming flow domains with contact lines. Computational results agree well with available experiments on transient fountain flow

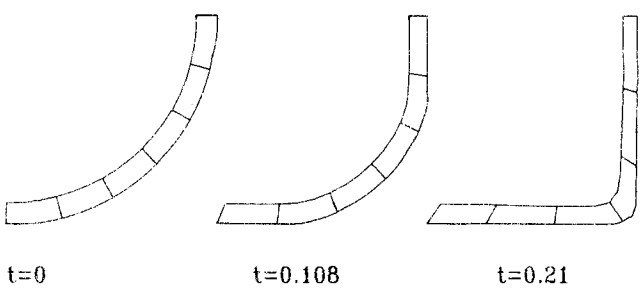

Figure 12. Magnification of fluid element shapes near flow front.

in a tube. Numerical tracking of material elements illustrates the rolling-type advancement of the fluid, V-shape formation, and stretching of the material parallel to the interface when two flow fronts collide to form a weldline.

Acknowledgment

Financial assistance from the Natural Sciences and Engineering Research Council of Canada is gratefully acknowledged. H. Mavridis was also the recipient of a Shell Canada Graduate Research Fellowship.

Notation

Ca = capillary number, $\mu U/\gamma$
e = unit vector
g = gravitational acceleration
g = unit body force vector
h = free-surface position parameter
$2H$ = mean surface curvature
i = unit vector in x direction
I = unit tensor
j = unit vector in y direction
J = Jacobian matrix
L = characteristic length scale
n = outward unit normal vector
P = pressure
P_a = ambient pressure
R = residual
Re = Reynolds number, $\rho UL/\mu$
s = arc length
S = Stokes number, $\mu U/\rho gL^2$
t = time
U = characteristic velocity scale
V = vector of nodal velocities
v = velocity vector
x = position vector
x, y = coordinate directions
X = vector of unknowns
Z = axial coordinate

Greek letters

γ = surface tension
δ = orientation angle for free-surface spines
η, ξ = local coordinates
θ = contact angle
μ = viscosity
π^i = pressure basis function
σ = total stress tensor
τ = deviatoric stress tensor
ϕ^i = velocity basis function

Superscript

i = quantity associated with ith node

Subscripts

B = base point
C = continuity
CL = contact line
F = free surface
FT = front tip
K = kinematic condition
m = momentum
w = wall
δ = midside spine direction

Literature Cited

Ballman, R. L., and H. L. Toor, "Orientation in Injection Molding," *Modern Plastics*, **38**, 113 (Oct., 1960).

Banthia, V., "Singularity of Collapsed Q-8 Finite Element," *Int. J. Num. Meth. Eng.*, **21**, 959 (1985).

Behrens, R. A., "Transient Domain Free Surface Flows and their Applications to Mold Filling," *Ph.D. Thesis*, Univ. Delaware (1983).

Behrens, R. A., M. J. Crochet, C. D. Denson, and A. B. Metzner, "Transient Free Surface Flows: Motion of a Fluid Advancing in a Tube," *AIChE J.*, **33**, 1178 (1987).

Beris, A. N., "Fluid Elements Deformation Behind an Advancing Flow Front," *J. Rheol.*, **31**, 121 (1987).

Chu, E., S. K. Goyal, and M. R. Kamal, "Prediction of Microstructure Development During Injection Mold Filling (The McKam-II Model)," *SPE ANTEC Tech. Papers*, **45**, 280 (1987).

Coyle, D. J., J. W. Blake, and C. W. Macosko, "The Kinematics of Fountain Flow in Mold Filling," *AIChE J.*, **33**, 1168 (1987).

Dussan, V., E. B., "On the Spreading of Liquids on Solid Surfaces: Static and Dynamic Contact Lines," *Ann. Rev. Fluid Mech.*, **11**, 371 (1979).

Gresho, P. M., R. L. Lee, and R. L. Sani, "On the Time-Dependent Solution of the Incompressible Navier-Stokes Equations in Two and Three Dimensions," *Recent Advances in Numerical Methods in Fluids*, v. 1, C. Taylor, K. Morgan, eds., Pineridge Press, Swansea, U.K. (1979).

Hagerman, E. M., "Weld-line Fracture in Molded Parts," *Plastics Eng.*, **29**, 67 (1974).

Huh, C., and L. E. Scriven, "Hydrodynamic Model of Steady Movement of a Solid/Liquid/Fluid Contact Line," *J. Colloid Interf. Sci.*, **35**, 85 (1971).

Keunings, R., "An Algorithm for the Simulation of Transient Viscoelastic Flows with Free Surfaces," *J. Comput. Phys.*, **62**, 199 (1986).

Kheshgi, H., and L. E. Scriven, "Penalty Finite-Element Analysis of Unsteady Free Surface Flows," *Finite Elements in Fluids*, v. 5, R. H. Gallagher et al., eds., 393 (1984).

Kistler, S. F., "The Fluid Mechanics of Curtain Coating and Related Viscous Free Surface Flows with Contact Lines," Ph.D. Thesis, Univ. Minnesota, Minneapolis (1984).

Kistler, S. F., and L. E. Scriven, "Coating Flows," *Computational Analysis of Polymer Processing*, J. R. A. Pearson, S. M. Richardson, eds., Applied Science Pub., London, New York (1983).

Lynch, D. R., "Unified Approach to Simulation on Deforming Elements with Application to Phase Change Problems," *J. Comput. Phys.*, **47**, 387 (1982).

Mavridis, H., A. N. Hrymak, and J. Vlachopoulos, "Finite-Element Simulation of Fountain Flow in Injection Molding," *Polym. Eng. Sci.*, **26**, 449 (1986a).

———, "Deformation and Orientation of Fluid Elements Behind an Advancing Flow Front," *J. Rheol.*, **30**, 555 (1986b).

Michael, D. H., "The Separation of a Viscous Liquid at a Straight Edge," *Mathematika*, **5**, 82 (1958).

Pismen, L. M., and A. Nir, "Motion of a Contact Line," *Phys. Fluids*, **25**, 3 (1982).

Rose, W., "Fluid-Fluid Interfaces in Steady Motion," *Nature*, **191**, 242 (1961).

Saito, H., and L. E. Scriven, "Study of Coating Flow by the Finite-Element Method," *J. Comput. Phys.*, **42**, 53 (1981).

Sang-Gook, K., and N. P. Suh, "Performance Prediction of Weldline Structure in Amorphous Polymers," *Polym. Eng. Sci.*, **26**, 1200 (1986).

Schmidt, L. R., "A Special Mold and Tracer Technique for Studying Shear and Extensional Flows in a Mold Cavity During Injection Molding," *Polym. Eng. Sci.*, **14**, 797 (1974).

Tadmor, Z., "Molecular Orientation in Injection Molding," *J. Appl. Polym. Sci.*, **18**, 1753 (1974).

Viriyayuthakorn, M., and R. V. Deboo, "A Finite-Element Model for Cable Jacketing Simulation," *SPE ANTEC Tech. Papers*, **41**, 178 (1983).

White, J. L., and W. Dietz, "Some Relationships Between Injection Molding Conditions and the Characteristics of Vitrified Molded Parts," *Polym. Eng. Sci.*, **19**, 1081 (1979).

Manuscript received July 29, 1987, and revision received Nov. 23, 1987.